4880 *Chem. Mater.* **2009,** *21,* 4880–4891
DOI:10.1021/cm901906e

CHEMISTRY OF MATERIALS
Article

# Origin of activation of Lattice Oxygen and Synergistic Interaction in Bimetal-Ionic $Ce_{0.89}Fe_{0.1}Pd_{0.01}O_{2-\delta}$ Catalyst

Asha Gupta,[†] Anil Kumar,[‡] Umesh V. Waghmare,[‡] and M. S. Hegde*[,§]

[†]*Materials Research Centre, Indian Institute of Science, Bangalore 560012, India,* [‡]*Theoretical Sciences Unit, Jawaharlal Nehru Centre for Advanced Scientific Research, Bangalore 560064, India, and* [§]*Solid State and Structural Chemistry Unit, Bangalore 560012, India*

*Received June 30, 2009. Revised Manuscript Received August 27, 2009*

Flourite-type nanocrystalline $Ce_{0.9}Fe_{0.1}O_{2-\delta}$ and $Ce_{0.89}Fe_{0.1}Pd_{0.01}O_{2-\delta}$ solid solutions have been synthesized by solution combustion method, which show higher oxygen storage/release property (OSC) compared to $CeO_2$ and $Ce_{0.8}Zr_{0.2}O_2$. Temperature programmed reduction and XPS study reveal that the presence of Pd ion in $Ce_{0.9}Fe_{0.1}O_{2-\delta}$ facilitates complete reduction of $Fe^{3+}$ to $Fe^{2+}$ state and partial reduction of $Ce^{4+}$ to $Ce^{3+}$ state at temperatures as low as 105 °C compared to 400 °C for monometal-ionic $Ce_{0.9}Fe_{0.1}O_{2-\delta}$. $Fe^{3+}$ ion is reduced to $Fe^{2+}$ and not to $Fe^0$ due to favorable redox potential for $Ce^{4+} + Fe^{2+} \rightarrow Ce^{3+} + Fe^{3+}$ reaction. Using first-principles density functional theory calculation we determine M−O (M = Pd, Fe, Ce) bond lengths, and find that bond lengths vary from shorter (2.16 Å) to longer (2.9 Å) bond distances compared to mean Ce−O bond distance of 2.34 Å for $CeO_2$. Using these results in bond valence analysis, we show that oxygen with bond valences as low as −1.55 are created, leading to activation of lattice oxygen in the bimetal ionic catalyst. Temperatures of CO oxidation and NO reduction by $CO/H_2$ are lower with the bimetal-ionic $Ce_{0.89}Fe_{0.1}Pd_{0.01}O_{2-\delta}$ catalyst compared to monometal-ionic $Ce_{0.9}Fe_{0.1}O_{2-\delta}$ and $Ce_{0.99}Pd_{0.01}O_{2-\delta}$ catalysts. From XPS studies of Pd impregnated on $CeO_2$ and $Fe_2O_3$ oxides, we show that the synergism leading to low temperature activation of lattice oxygen in bimetal-ionic catalyst $Ce_{0.89}Fe_{0.1}Pd_{0.01}O_{2-\delta}$ is due to low-temperature reduction of $Pd^{2+}$ to $Pd^0$, followed by $Pd^0 + 2Fe^{3+} \rightarrow Pd^{2+} + 2Fe^{2+}$, $Pd^0 + 2Ce^{4+} \rightarrow Pd^{2+} + 2Ce^{3+}$ redox reaction.

## 1. Introduction

The amount of oxygen that can be reversibly exchanged from the lattice is defined as oxygen storage capacity (OSC).[1] OSC is one of the important properties required for three-way catalysis in order to remove harmful CO from autoexhaust. $CeO_2$, a reducible oxide with fluorite structure, has become the main component of three-way catalyst (TWC) because of its oxygen storage/release capacity (OSC)

$$CeO_2 + \delta CO \rightarrow CeO_{2-\delta} + \delta CO_2 \text{ and}$$

$$CeO_{2-\delta} + \frac{\delta}{2} O_2 \rightarrow CeO_2$$

Thus, $CeO_2$ provides a buffer against considerable oscillation in air-to-fuel ratio and guarantees good performance as potential TWCs.[1,2] $CeO_2$ is one of the most stable lattices and the fluorite structure is retained even with large amount of oxygen deficiency. However, the amount of lattice oxygen taking part in the redox reactions is small ($\delta \approx 0.05$) and further improvement of the OSC of $CeO_2$ for practical use has led to development of new $CeO_2$-based oxygen storage materials.[3] Substitution of Zr, Ti, Sn in $CeO_2$ in the form of solid solution of $Ce_{1-x}M_xO_2$ (M = Zr, Ti, Sn) is known to increase the OSC of $CeO_2$.[4−9] Ce in $CeO_2$ has 8-fold coordination with all Ce−O bond length equal to 2.34 Å. Substitution of smaller ions like $Zr^{4+}$ (ionic radii, $r = 0.84$ Å) and $Ti^{4+}$ ($r = 0.74$ Å) for $Ce^{4+}$ ions ($r = 0.99$ Å) distorts the local 8-fold coordination around the dopant site, and these smaller ions, therefore, prefer coordination numbers smaller than eight. EXAFS and DFT studies reported by Dutta et al.[10] have shown that both Ce and Zr exhibit tetrahedral-like 4 + 4 coordination in $Ce_{1-x}Zr_xO_2$. Similar results were observed for $Ce_{1-x}Ti_xO_2$ solid solution where both Ti and Ce ions preferred 4 + 4 coordination.[8] Because of this

*Corresponding author. Fax: +91 80 2360 1310. E-mail: mshegde@sscu.iisc.ernet.in.

(1) Yao, H. C.; Yao, Y. F. Y. *J. Catal.* **1984**, *86*, 254.
(2) Trovarelli, A. *Catalysis by Ceria and Related Materials*; Imperial College Press, London, 2002.
(3) Trovarelli, A.; deLeitenburg, C.; Dolcetti, G. *CHEMTECH* **1997**, *27*, 32.
(4) Baidya, T.; Hegde, M. S.; Gopalakrishnan, J. *J. Phys. Chem. B* **2007**, *111*, 5149.
(5) Nagai, Y.; Yamamoto, T.; Tanaka, T.; Yoshida, S.; Nonaka, T.; Okamoto, T.; Suda, A.; Sugiura, M. *Catal. Today* **2002**, *74*, 225.
(6) Vlaic, G.; Fornasiero, P.; Geremia, S.; Kaspar, J.; Graziani, M. *J. Catal.* **1997**, *168*, 386.
(7) Baidya, T.; Priolkar, K. R.; Sarode, P. R.; Hegde, M. S.; Asakura, K.; Tateno, G.; Koike, Y. *J. Chem. Phys.* **2008**, *128*, 124711.
(8) Dutta, G.; Waghmare, U. V.; Baidya, T.; Hegde, M. S.; Priolkar, K. R.; Sarode, P. R. *Chem. Mater.* **2006**, *18*, 3249.
(9) Baidya, T.; Gupta, A.; Deshpandey, P. A.; Madras, G.; Hegde, M. S. *J. Phys. Chem. C* **2009**, *113*, 4059.
(10) Dutta, G.; Waghmare, U.; Baidya, T.; Hegde, M.; Priolkar, K.; Sarode, P. *Catal. Lett.* **2006**, *108*, 165.

 Published on Web 10/02/2009 

distortion of the oxygen sublattice, in $Ce_{1-x}Ti_xO_2$ for example, four of the Ti−O and Ce−O bonds became longer than in $TiO_2$ and $CeO_2$ respectively. The oxygen with longer Ce−O and Ti−O bonds can be extracted by CO or $H_2$ at a lower temperature. The oxygen with longer (Ce, Ti)-O bonds can be defined as activated oxygen in the $Ce_{1-x}Ti_xO_2$ lattice, which is responsible for higher OSC. The concept of activation of oxygen was also reported by Metiu and co-workers, where they have shown that dopant atom weakens the surrounding oxygen bond of the doped oxide, making it a better oxidant and thus facilitating CO oxidation.[11,12]

Although substitution of Zr, Ti, Sn increased OSC, the activity of the catalyst is poor at low temperatures. In contrast, noble metal ions like Pd, Pt, Ru, Rh substitution in $CeO_2$ show high CO oxidation rates at low temperatures,[13] and the OSC of such catalysts is small. The high CO conversion rates at low temperatures are attributed to the availability of noble metal ion sites for CO adsorption. The OSC material, which finds application in auto-exhaust, needs to be promoted by noble metal ions substitution for good performance and high activity at low temperature. Yet another application of oxygen storage materials is the generation of hydrogen fuel via the water−gas shift reaction

$$Ce_{1-x}Ti_xO_2+\delta CO \rightarrow Ce_{1-x}Ti_xO_{2-\delta}+\delta CO_2$$

$$Ce_{1-x}Ti_xO_{2-\delta}+\delta H_2O \rightarrow Ce_{1-x}Ti_xO_2+\delta H_2$$

The rates of $H_2$-generation was increased by $Pt^{2+}$ ion substitution in the catalyst where $Pt^{2+}$ ion provided CO adsorption sites.[14] Hence, fabrication of such high OSC materials activated with noble metal ions substitution for practical applications and understanding the electronic and structural origin of their catalytic activity is essential to development of TWCs.

Substitution of transition metal like Cr,[15] Mn,[16] Fe[17] in $CeO_2$ in fluorite structure shows high OSC and brings down the cost of the catalyst considerably. However, the mechanism behind high OSC of these catalysts has not been understood. Keeping this in mind, we have synthesized $Ce_{0.9}Fe_{0.1}O_{2-\delta}$ and $Ce_{0.89}Fe_{0.1}Pd_{0.01}O_{2-\delta}$ by the solution combustion method, and indeed found that lattice oxygen is highly activated in $Ce_{0.89}Fe_{0.1}Pd_{0.01}O_{2-\delta}$, leading to high OSC and high CO oxidation activity at low temperatures. From a detailed experimental study combined with DFT calculations and bond-valence analysis, we show that (a) destabilization of lattice oxygen sublattice due to longer M−O bonds in bimetal-ionic catalyst than Ce−O bonds in $CeO_2$ is responsible for high OSC and (b) the synergistic electronic interaction between $Pd^0$ and $Ce^{4+}$ and $Fe^{3+}$ states is responsible for enhanced low temperature activation of lattice oxygen.

## 2. Methods

**2.1. Experimental Section.** $Ce_{0.9}Fe_{0.1}O_{2-\delta}$ and $Ce_{0.89}Fe_{0.1}Pd_{0.01}O_{2-\delta}$ were prepared by solution combustion method using glycine as a fuel. In an typical preparation, 5.4826 g (0.01 mol) of ceric ammonium nitrate, $(NH_4)_2Ce(NO_3)_6$ (Loba Chemie), 0.449 g (0.0011 mol) of ferric nitrate [$Fe(NO_3)_3.9H_2O$, Aldrich] and 2.14 g of (0.0285 mol) glycine [$C_2H_5O_2N$, Aldrich] was taken in a crystallizing dish, and dissolved in a minimum volume of water to obtain a clear solution. The dish was then transferred to a preheated furnace kept at 350 °C. After dehydration, the whole mass catches fire and solid solution of $Ce_{1-x}Fe_xO_{2-\delta}$ is formed within 5 min. For 1 (and 2) at % Pd substituted $Ce_{1-x}Fe_xO_{2-\delta}$, the following weights were taken: 5.4826 g of ceric ammonium nitrate, 0.454 g (and 0.46 g) of ferric nitrate, 0.02 g (and 0.04 g) of palladium chloride ($PdCl_2$, Aldrich), and 2.14 g of glycine. The color of Fe-substituted catalyst is red; on Pd substitution, the color becomes slightly darker.

For further experimental requirements, 3 at % Pd-metal impregnated on $CeO_2$ and on $Fe_2O_3$ were also synthesized. Pure $CeO_2$ and $Fe_2O_3$ were first prepared by solution combustion method using glycine and urea as fuel respectively. Impregnation of Pd-metal was carried out by dispersing the oxides in dilute solution of $PdCl_2$, followed by addition of dilute hydrazine hydrate solution. So the reduced Pd-metal is deposited on the surface of the oxide, the samples were then dried at 150 °C for 3 h.

The products were characterized by powder X-ray diffraction (XRD) (Philips X'Pert Diffractometer fitted with graphite crystal postmonochromator, Cu Kα radiation). Structures were refined by the Rietveld method on the $CeO_2$ fluorite model by means of Fullprof program.[18] For this purpose, XRD data were collected at a scan rate of 0.25° $2\theta$ $min^{-1}$ with 0.01° step size in the $2\theta$ range between 20 and 90°. For Transmission electron microscopy (TEM) studies, a acetone dispersion of the sample was dropped onto holey carbon coated Cu grids and the images were recorded with FeI Technai 20 instrument at 200 kV. X-ray photoelectron spectra (XPS) were recorded on a Thermoscientific Multilab 2000 equipment employing Al Kα X-rays. XPS binding energies are accurate within ±0.1 eV.

Oxygen storage/release properties of solid catalyst were studied by hydrogen uptake measurements carried out in a microreactor (30 cm length and 0.4 cm internal diameter) employing 5.49% $H_2$/Ar (certified calibration gases mixture obtained from Chemix Specialty Gases and Equipment, Bangalore, India) with 30 sccm flow rate and 10 °C/min linear heating rate up to 550 °C. Volume of hydrogen intake/consumption by the sample was calibrated against CuO standard using an online thermal conducting detector (TCD). After the first cycle, the catalyst was cooled in $H_2$/Ar to room temperature. The catalyst was then reoxidized at 400 °C for 1 h in $O_2$ and cooled to room temperature in $O_2$, and a second temperature-programmed reaction (TPR) run was carried out. Similar consecutive TPR runs were carried out for several cycles.

(11) Chrétien, S.; Metiu, H. *Catal. Lett*. **2006**, *107*, 143.
(12) Nolan, M.; Verdugo, V. S.; Metiu, H. *Surf. Sci*. **2008**, *602*, 2734.
(13) Hegde, M. S.; Madras, G.; Patil, K. C. *Acc. Chem. Res*. **2009**, *42*, 704.
(14) Sharma, S.; Deshpande, P. A.; Hegde, M. S.; Madras, G. *Ind. Eng. Chem. Res*. **2009**, *48*, 6535.
(15) Singh, P.; Hegde, M. S.; Gopalakrishnan, J. *Chem. Mater*. **2008**, *20*, 7268.
(16) Murugan, B.; Ramaswamy, A. V.; Srinivas, D.; Gopinath, C. S.; Ramaswamy, V. *Chem. Mater*. **2005**, *17*, 3983.
(17) Singh, P.; Hegde, M. S. *J. Solid State Chem*. **2008**, *181*, 3248.
(18) Rodriguez-Carvajal, J. *Multi-pattern Rietveld Refinement Program Fullprof 2k, version 3.30*; Laboratoire Leon Brillouin, Institut Laue Langevin: Saclay, France, 2005.

The catalytic test was done in a temperature-programmed reaction system described elsewhere.[19] The catalyst (40/80 mesh) diluted with $SiO_2$ (30/60 mesh size) was loaded in the reactor to get a column length of 1.1 cm and the endings were plugged with ceramic wool. For all the reactions, the total flow was kept fixed at 100 sccm with helium gas as the balance to achieve a gas hourly space velocity (GHSV) of 43 000 $h^{-1}$. Noncatalytic CO oxidation (CO/TPR) was carried out by passing 1 vol % CO balanced with He over 150 mg of the catalyst. Catalytic CO oxidation was carried out under excess oxygen; the feed gas composition was 1 vol % CO and 1 vol % $O_2$ with He as the balance over 100 mg of catalyst. NO reduction by CO was carried out under stoichiometric condition with 1 vol % CO and 1 vol % NO with a total flow of 100 sccm over 100 mg of catalyst. NO reduction by $H_2$ over 100 mg of catalysts was carried out with the inlet gas composition of $NO:H_2 = 0.5:1$ vol %.

**2.2. Computational.** First-principles calculations are based on density functional theory (DFT) with a local density approximation (LDA) to the exchange correlation energy of electrons. Interaction between valence electrons and ionic cores is treated using first-principles ultrasoft pseudopotentials[20] known for their high efficiency in calculating the structural and electronic properties. Semicore states of Ce, Fe, Pd and O are included in the valence and spin polarization is not considered in our calculation. We used PWSCF[21] implementation of DFT to optimize the internal structure to minimize the total energy. A $2 \times 2 \times 2$ (with 96-atoms) supercell built from the conventional cubic unit cell was used in the simulation of solid-solutions, which contains 32 formula units of $CeO_2$. The integrals over the Brillouin zone was sampled on $4 \times 4 \times 4$ $k$-point Monkhorst-Pack.[22]

Bond-lengths determined from the optimized structures are used to calculate bond-valence of metal ions following the bond valence method described by I. D. Brown and M. O'Keeffe.[23] Bond valence is defined as: $s = \exp[-(R - R_0)/B]$, where $R$ is the bond length, $R_0$ is the length of a bond of unit valence, and $B$ is the fitted parameter.

## 3. Results and Discussion

**3.1. XRD Study.** The X-ray diffraction lines of $Ce_{0.9}Fe_{0.1}O_{2-\delta}$ and $Ce_{0.89}Fe_{0.1}Pd_{0.01}O_{2-\delta}$, shown in Figure 1a, could be indexed to the fluorite structure of ceria. The XRD patterns were magnified by 10 times in the $y$-scale (Figure 1b) with respect to the $CeO_2$ (111) peak, and diffraction lines corresponding to FeO, $Fe_2O_3$, or $Fe_3O_4$ are not observed, implying substitution of Fe in $CeO_2$. However, it is difficult to detect Pd-metal or PdO in the XRD pattern at 1 at % level.

The XRD patterns were Rietveld refined by simultaneously varying 18 parameters that include the overall scale factor, background parameters, unit cell, half width, shape, and isotropic thermal parameters along with the oxygen occupancy. $Fe^{3+}$ and $Pd^{2+}$ ions are taken in $Ce^{4+}$ sites. Pseudo-Voigt function was used as profile

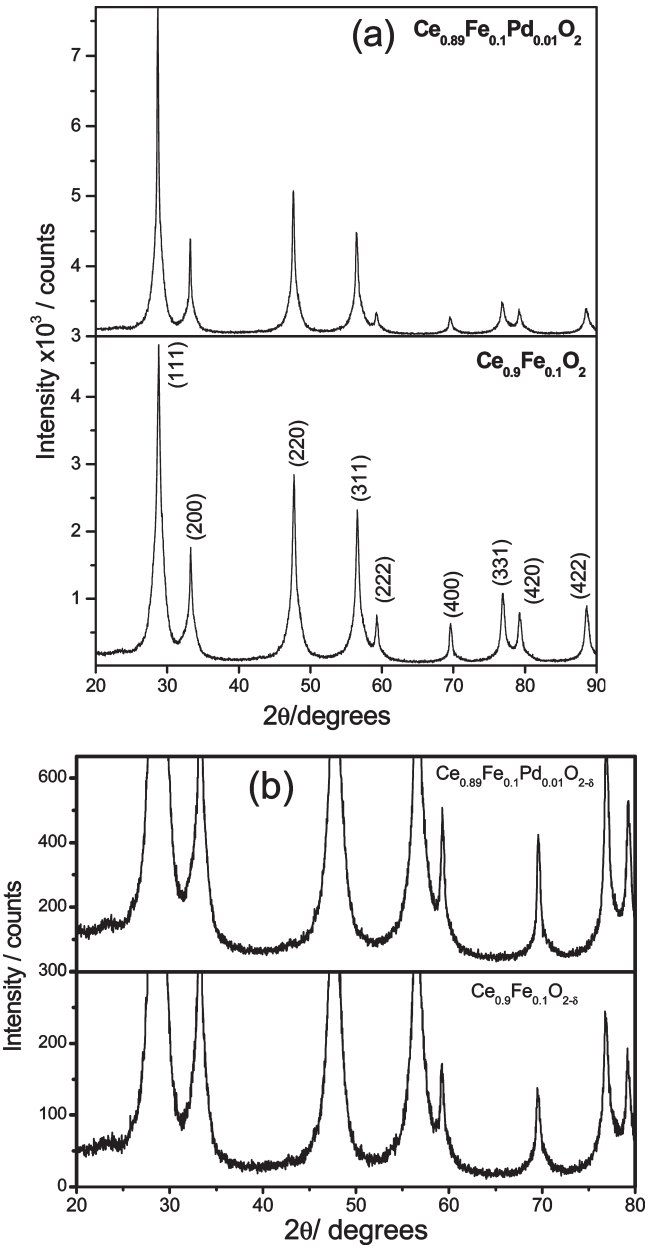


**Figure 1.** (a) XRD patterns of $Ce_{0.9}Fe_{0.1}O_{2-\delta}$ and $Ce_{0.89}Fe_{0.1}Pd_{0.01}O_{2-\delta}$, (b) XRD patterns magnified 10 times in $y$-scale.

parameter for peak width analysis. The refined X-ray profiles fit well with the observed X-ray data (Figure 2). Crystallite sizes were estimated by using the Scherrer formula[24]

$$\text{crystallite size } (d) = \frac{0.9\lambda}{\beta \cos\theta} \quad (1)$$

where $\lambda$ is the wavelength of the X-ray, $\beta$ is the full width at half maxima (fwhm) in radians, and $\theta$ is the diffraction angle. fwhm was estimated taking the $U$, $V$, $W$ values from the Rietveld refinement data given by the equation[25]

$$\beta = (U\tan^2\theta + V\tan\theta + W)^{1/2} \quad (2)$$

(19) Gayen, A.; Baidya, T.; Ramesh, G. S.; Srihari, R.; Hegde, M. S. *J. Chem. Sci.* **2006**, *118*, 9.
(20) Vanderbilt, D. *Phys. Rev. B: Condens. Matter Mater. Phys.* **1990**, *41*, 7892.
(21) Baroni, S.; Dal Corso, A.; de Gironcoli, S.; Giannozzi, P. http://www.pwscf.org.
(22) Monkhorst, H. J.; Pack, J. D. *Phys. Rev. B* **1976**, *13*, 5188.
(23) Brown, I. D. The Bond-Valence Method: An Empirical Approach to Chemical Structure and Bonding. In *Structure and Bonding in Crystals*; O'Keeffe, M., Navrotsky, A., Eds.; Academic Press: New York, 1981; Vol. *2*.
(24) Cullity, B. D. *Elements of X-ray Diffraction*, 2nd ed.; Addison-Wesley: Reading, MA, 1978.
(25) Caglioti, G.; Paoletti, A.; Ricci, F. P. *Nucl. Instrum.* **1958**, *3*, 223.

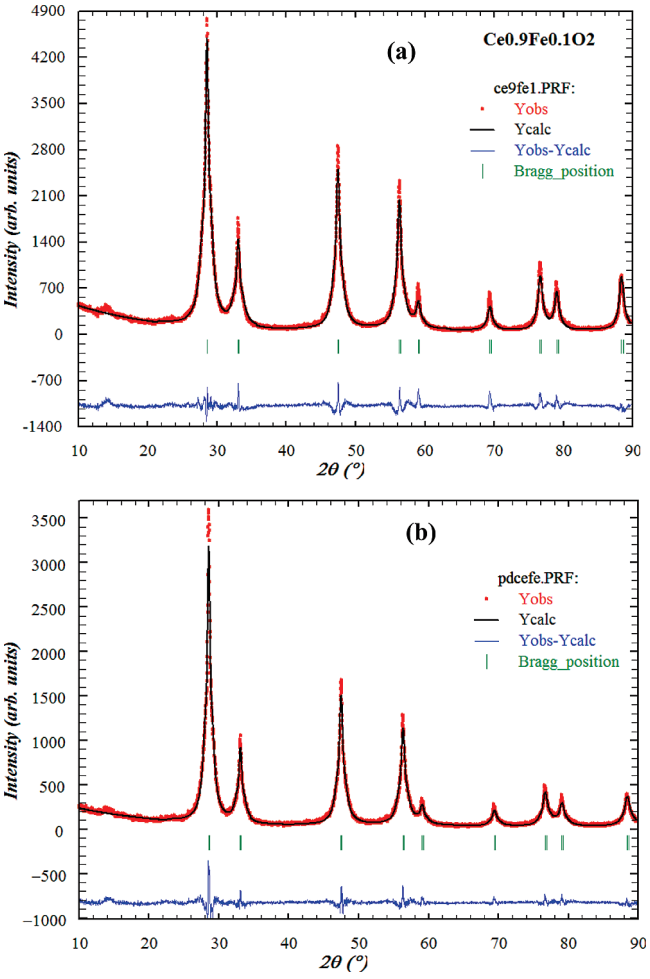


**Figure 2.** Rietveld refined XRD pattern of as-prepared (a) $Ce_{0.9}Fe_{0.1}O_{2-\delta}$ and (b) $Ce_{0.89}Fe_{0.1}Pd_{0.01}O_{2-\delta}$.

**Table 1. Rietveld Refined Parameters of Pure $CeO_2$ and Fe- and Pd-Substituted $CeO_2$**

| catalyst | $a$ (Å) | $R_{Bragg}$ | $R_f$ | $\chi^2$ |
|---|---|---|---|---|
| $CeO_2$ | 5.4113 (3) | | | |
| $Ce_{0.9}Fe_{0.1}O_2$ | 5.4159 (5) | 1.78 | 1.71 | 2.34 |
| $Ce_{0.89}Fe_{0.1}Pd_{0.01}O_2$ | 5.4131 (4) | 1.81 | 1.42 | 2.01 |

The crystallite size calculated by this method is found to be 6 nm for both $Ce_{0.9}Fe_{0.1}O_{2-\delta}$ and $Ce_{0.89}Fe_{0.1}Pd_{0.01}O_{2-\delta}$. The lattice parameters, $R_{Bragg}$, $R_f$ and $\chi^2$ obtained from the refinement of pure $CeO_2$, $Ce_{0.9}Fe_{0.1}O_{2-\delta}$, and $Ce_{0.89}Fe_{0.1}Pd_{0.01}O_{2-\delta}$ are summarized in Table 1. Instead of a decrease in lattice parameter due to substitution of smaller $Fe^{3+}$ ions (ionic radii, $r = 0.645$ Å) for larger $Ce^{4+}$ ion ($r = 0.97$ Å), we see a slight increase in lattice parameter ($a = 5.4159(5)$ Å) compared to $CeO_2$ ($a = 5.411$ Å, JCPDS No. 340394). On $Pd^{2+}$ ion ($r = 0.86$ Å) substitution, there is a slight decrease in lattice parameter compared to $Ce_{0.9}Fe_{0.1}O_{2-\delta}$, indicating Pd ion substitution in the lattice.

**3.2. TEM Study.** High-resolution transmission electron micrograph (HRTEM) of $Ce_{0.89}Fe_{0.1}Pd_{0.01}O_{2-\delta}$ is shown in Figure 3. The average crystallite size is $5 \pm 1$ nm. Crystallite size from TEM agrees with those measured from Scherrer formula. Well-defined high-resolution image indicates that the particles are highly crystalline in nature and the presence of other phase is not observed. The selected area diffraction pattern given in the inset of Figure 3 is indexed to fluorite structure, and no other ring pattern is observed. Lattice fringes in the high-resolution TEM are at 3.1 Å corresponding to $d_{111}$ planes of the title compound.

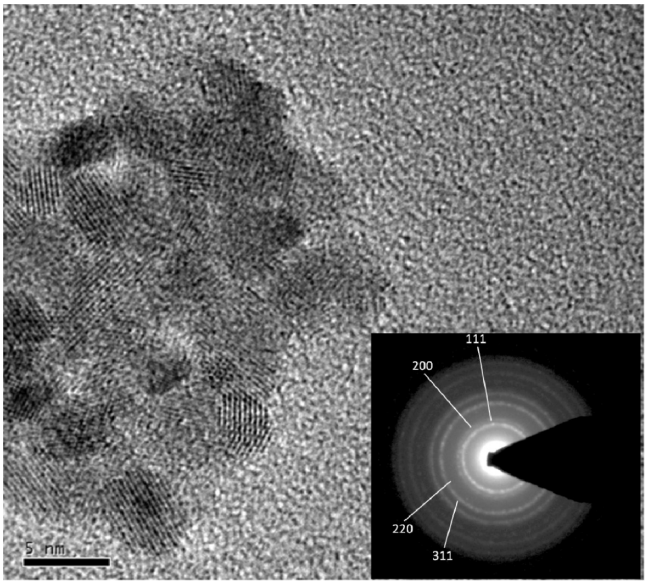


**Figure 3.** HRTEM $Ce_{0.89}Fe_{0.1}Pd_{0.01}O_{2-\delta}$ and diffraction pattern (inset) of $Ce_{0.89}Fe_{0.1}Pd_{0.01}O_{2-\delta}$.

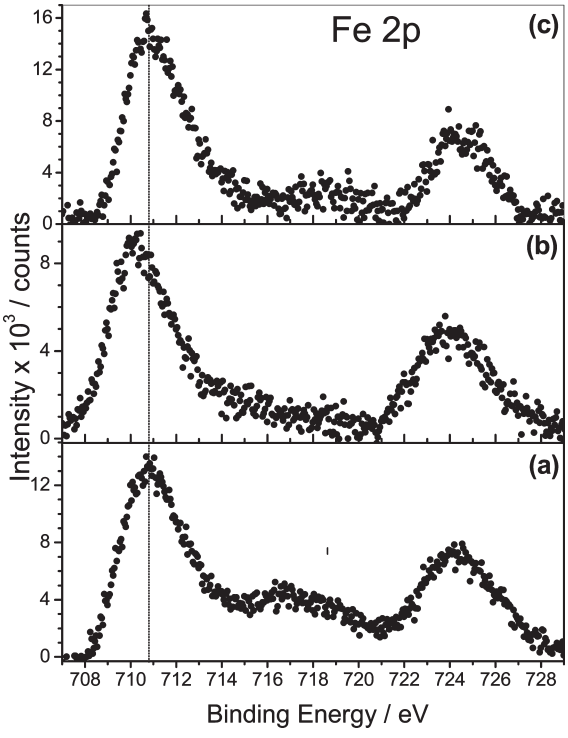


**Figure 4.** Fe 2p core level spectra of $Ce_{0.9}Fe_{0.1}O_{2-\delta}$: (a) as-prepared, (b) reduced in $H_2$ up to 550 °C, and (c) reoxidized in $O_2$ at 550 °C.

**3.3. XPS Study.** *3.3.1. $Ce_{0.9}Fe_{0.1}O_{2-\delta}$.* The binding energy of Fe($2p_{3/2,\ 1/2}$) core level of as prepared $Ce_{0.9}Fe_{0.1}O_{2-\delta}$ is observed at 710.8 and 724.2 eV, respectively (Figure 4a). A satellite peak appears at ~8 eV from the main $2p_{3/2}$ level, which matches with the literature

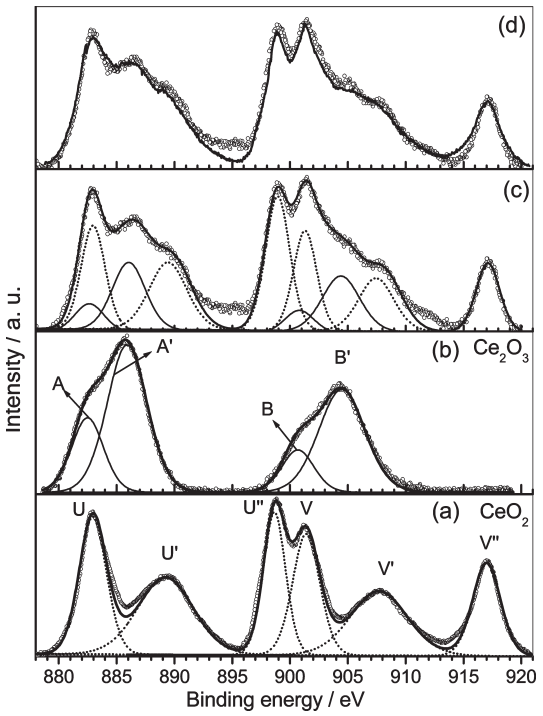


**Figure 5.** Ce (4f) core level spectra of (a) $CeO_2$, (b) $Ce_2O_3$. (c) Deconvoluted Ce (4f) core level spectra of $Ce_{0.89}Fe_{0.1}Pd_{0.01}O_{2-\delta}$ reduced in $H_2$ up to 550 °C, and (d) Fitted Ce (4f) core level spectra of $Ce_{0.89}Fe_{0.1}Pd_{0.01}O_{2-\delta}$ reduced in $H_2$ up to 550 °C; the bold envelope is obtained by adding 65% $CeO_2$ and 35% $Ce_2O_3$ spectra.

reported $Fe_2O_3$,[26−28] indicating that Fe is in +3 oxidation state in the as-prepared oxide catalyst. The red color of the catalyst also indicates that Fe is in the +3 oxidation state. Upon reduction of the same compound in $H_2$ up to 550 °C (Figure 4b), Fe($2p_{3/2,\ 1/2}$) peaks shift to lower binding energy at 709.9 and 723.6 eV, and the characteristic satellite due to the $Fe^{3+}$ state is absent. A small satellite peak is present at ∼5 eV from the main peak , which is characteristics of the $Fe^{2+}$ state as in FeO.[28] Upon reoxidation of the reduced oxide in $O_2$ flow at 550 °C, the Fe 2p reverts to $Fe^{3+}$ state as seen by the presence of the satellite peak, corresponding to the +3 state (Figue 4c).

To estimate the relative concentrations of $Ce^{3+}$ to $Ce^{4+}$ in our samples, the XPS of $CeO_2$ and $Ce_2O_3$ were recorded (Figure 5) and the characteristic satellites that are observed because of 3d core levels of $Ce^{4+}$ and $Ce^{3+}$ states are same as reported by Kotani et al.[29] Accordingly, Ce(3d) core levels of $CeO_2$ and $Ce_2O_3$ are deconvoluted into main and satellite peaks. The binding energy of Ce($3d_{5/2,\ 3/2}$) levels for $CeO_2$ are at 883 eV (marked U) and 901.3 eV (marked V) and their characteristics satellites peaks are marked U′, U″, V′, and V′ respectively. The Ce $3d_{5/2}$ and $3d_{3/2}$ peaks for $Ce_2O_3$ are at 882.5 eV (marked A) and 900.6 eV (marked B) and their corresponding satellites are marked A′ and B′, respectively.

When Ce is present in both +4 and +3 oxidation states as in $Ce_{0.89}Fe_{0.1}Pd_{0.01}O_{2-\delta}$ reduced in $H_2$ up to 550 °C (Figure 5c,d), the XP spectrum of Ce(3d) becomes complicated and estimation of the relative concentrations of $Ce^{3+}/Ce^{4+}$ becomes difficult. The spectrum can be resolved into $Ce^{3+}$ and $Ce^{4+}$ components taking the same relative intensities and half widths of the main band and satellite peaks as that observed in Figure 5a,b. The two spectra are normalized with respect to main $3d_{5/2}$ band and the total area under the peak $3d_{5/2}$ and $3d_{3/2}$ is used to determine the relative ratio of the two oxidation states. Figure 5c shows the deconvoluted spectra of Ce(3d) core level spectra of reduced $Ce_{0.89}Fe_{0.1}Pd_{0.01}O_{2-\delta}$ and the ratio of $Ce^{4+}$ to $Ce^{3+}$ was found to be 0.65:0.35. Another simpler approach could be to add the intensities of $CeO_2$ and $Ce_2O_3$ in the ratio 0.65:0.35 and the resultant spectra should match with the deconvoluted spectra. In Figure 5d the bold envelope is the spectra obtained by adding $CeO_2$ and $Ce_2O_3$ in the ratio 0.65:0.35, and there is close agreement between the observed and fitted spectra. This method of adding the individual spectra gives relative ratio of $Ce^{4+}/Ce^{3+}$ within 2−3% error compared to deconvoluted spectra, and we have used this method to determine the concentration of $Ce^{4+}$ and $Ce^{3+}$ henceforth.

The XPS of Ce($3d_{5/2,\ 3/2}$) of the as prepared $Ce_{0.9}Fe_{0.1}O_{2-\delta}$ catalyst shown in Figure 6(a) is found to have 85% Ce in +4 state and 15% in +3 oxidation state. Due to partial reduction of $Ce^{4+}$ ($r = 0.97$ Å) to $Ce^{3+}$ ($r =$ 1.23 Å), a slight increase in the lattice parameter $a$ is observed for $Fe^{3+}$ ion substituted compound (see Table 1). Ce(3d) spectra of $Ce_{0.9}Fe_{0.1}O_{2-\delta}$ reduced up

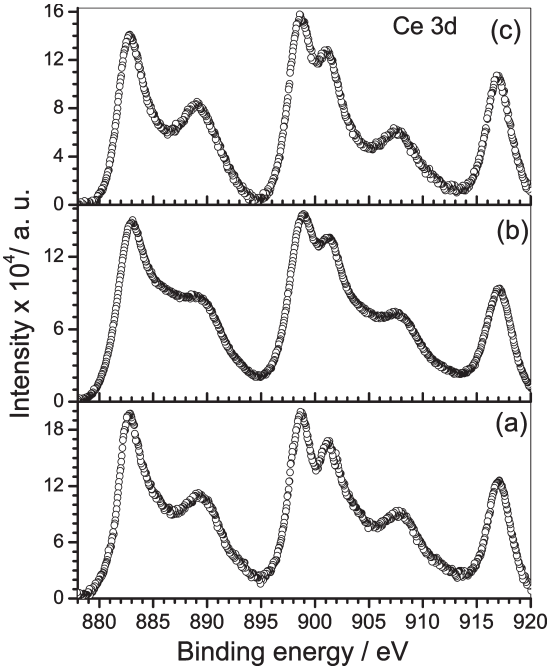


**Figure 6.** Ce 3d core level spectra respectively of $Ce_{0.9}Fe_{0.1}O_{2-\delta}$: (a) as-prepared, (b) reduced in $H_2$ up to 550 °C, and (c) reoxidized in $O_2$ at 550 °C.

(26) Grosvenor, A. P.; Kobe, B. A.; Biesinger, M. C.; McIntyre, N. S. *Surf. Interface Anal.* **2004**, *36*, 1564.
(27) Rao, C. N. R.; Sarma, D. D.; Vasudevan, S.; Hegde, M. S. *Proc. R. Soc. London, Ser. A* **1979**, *367*, 239.
(28) Yamashita, T.; Hayes, P. *Appl. Surf. Sci.* **2008**, *254*, 2441.
(29) Kotani, A.; Ogasawara, H. *J. Electron Spectrosc. Relat. Phenom.* **1992**, *60*, 257.

**Table 2. Composition from XPS of As-Prepared and Reduced Samples**

| | at 260 °C | | at 550 °C | |
|---|---|---|---|---|
| composition of as-prepared compound from XPS | reduced composition | OSC in $\mu$mol g$^{-1}$ | reduced composition | OSC in $\mu$mol g$^{-1}$ |
| $Ce^{4+}_{0.76}Ce^{3+}_{0.14}Fe^{3+}_{0.1}O_{1.88}$ | | | $Ce^{4+}_{0.64}Ce^{3+}_{0.26}Fe^{2+}_{0.1}O_{1.77}$ (TPR)<br>$Ce^{4+}_{0.67}Ce^{3+}_{0.23}Fe^{2+}_{0.1}O_{1.79}$ (XPS) | 665 |
| $Ce^{4+}_{0.69}Ce^{3+}_{0.2}Fe^{3+}_{0.1}Pd^{2+}_{0.01}O_{1.84}$ | $Ce^{4+}_{0.63}Ce^{3+}_{0.26}Fe^{2+}_{0.1}Pd^{0}_{0.01}O_{1.75}$ (TPR)<br>$Ce^{4+}_{0.63}Ce^{3+}_{0.26}Fe^{2+}_{0.1}Pd^{0}_{0.01}O_{1.75}$ (XPS) | 592 | $Ce^{4+}_{0.55}Ce^{3+}_{0.34}Fe^{2+}_{0.1}Pd^{0}_{0.01}O_{1.71}$ (TPR)<br>$Ce^{4+}_{0.58}Ce^{3+}_{0.31}Fe^{2+}_{0.1}Pd^{0}_{0.01}O_{1.73}$ (XPS) | 780 |

to 550 °C (Figure 6b) has 75% $Ce^{4+}$ and 25% $Ce^{3+}$ ion. On reoxidation, Ce shows a higher percentage of the +4 oxidation state (90% $Ce^{4+}$ and 10% $Ce^{3+}$) compared to the as-prepared compound (Figure 6c).

In the as-prepared oxide, catalyst Fe is present in the +3 oxidation state and 85% Ce is in the +4 oxidation state; the composition of the as-prepared compound is given by $Ce^{+4}_{0.76}Ce^{+3}_{0.14}Fe^{+3}_{0.1}O_{1.88}$. When the sample is reduced in $H_2$ at 550 °C, complete reduction of $Fe^{3+}$ to $Fe^{2+}$ takes place and partial reduction of $Ce^{4+}$ to $Ce^{3+}$ also occurs; the formula of the reduced $Ce_{0.9}Fe_{0.1}O_{2-\delta}$ sample is given by $Ce^{+4}_{0.68}Ce^{+3}_{0.22}Fe^{+3}_{0.1}O_{1.79}$. The formulas of the as-prepared and reduced catalysts are summarized in Table 2. It should be noted that the $Fe^{3+}$ ion is reduced only to +2 oxidation state, and further reduction to $Fe^0$ does not occur.

An estimation of relative concentration of Ce and Fe of as prepared and reduced catalyst was carried out from the intensities of Fe(2p) and Ce(3d) peaks:[30]

$$\text{concentration, } C_M = \frac{\frac{I_M}{\lambda_M \sigma_M D_M}}{\Sigma\left(\frac{I_M}{\lambda_M \sigma_M D_M}\right)} \quad (3)$$

where $I_M$ is the integrated intensity of the core levels (M = Ce(3d), Fe(2p)) $\lambda_M$ is the mean escape depths of the respective photoelectrons, $\sigma_M$ is the photoionization cross section, and $D_M$ is the geometric factor. The photoionization cross-section values were taken from Scofield,[31] and mean escape depths were taken from Penn.[32] The geometric factor was taken as 1, because the maximum intensity in this spectrometer is obtained at 90°. Accordingly, for as-prepared sample, the surface composition of Ce and Fe were 0.88 and 0.12 compared to the bulk composition of 0.9 and 0.1 taken in the preparation. Upon reoxidation of the reduced sample at 550 °C, the ratio remains same at 0.88 and 0.12. Thus, the surface composition of Ce and Fe are close to the bulk composition.

*3.3.2. $Ce_{0.89}Fe_{0.1}Pd_{0.01}O_{2-\delta}$.* The binding energy of Fe($2p_{3/2, 1/2}$) core level spectra of as prepared $Ce_{0.89}Fe_{0.1}Pd_{0.01}O_{2-\delta}$ is observed at 710.8 and 724.2 eV (Figure 7a) corresponding to the +3 oxidation state of Fe. On $H_2$ reduction up to 250 °C, Fe($2p_{3/2}$) peak shifts to lower binding energy at 709.9 eV (Figure 7b), corresponding to Fe in +2 state. On further reduction to higher temperature up to 550 °C, no shift of $2p_{3/2}$ peak is observed

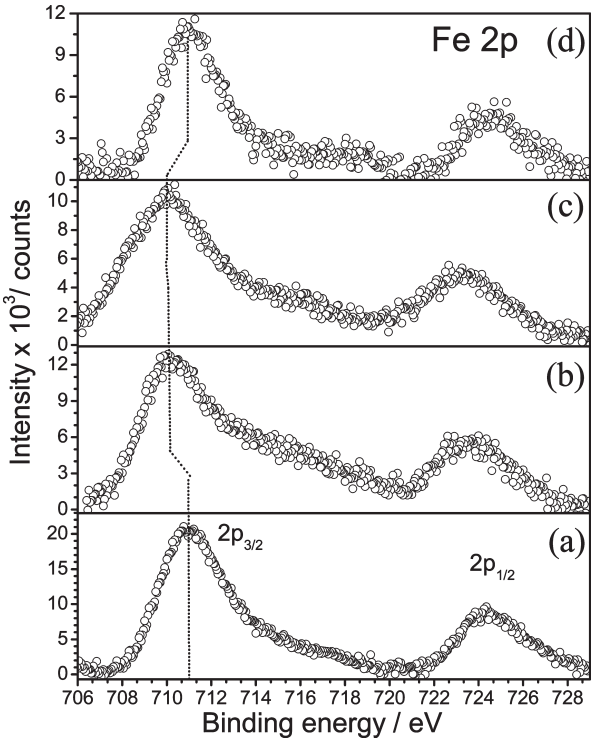


**Figure 7.** Fe 2p core level spectra $Ce_{0.89}Fe_{0.1}Pd_{0.01}O_{2-\delta}$: (a) as-prepared sample, reduced in $H_2$ up to (b) 260 °C, (c) 550 °C, and (d) reoxidized at 550 °C in $O_2$.

(Figure 7c). Upon oxidation of the reduced sample in $O_2$ at 550 °C, Fe completely gets oxidized to +3 state (Figure 7d).

Binding energy of Pd($3d_{5/2}$) is observed at 337.2 eV (Figure 8a) indicating that Pd is present in $Pd^{2+}$ state in as prepared catalyst.[33] The sample was then reduced in $H_2$ at 250 °C; the color of the reduced sample was black. Even with all precautions, while transferring the reduced sample to XPS chamber, the surface was seen to regain the original color partly, indicating that the sample got partly oxidized. The Pd(3d) core level spectrum (Figure 8b) shows a broad peak at 337.2 eV and a shoulder at 335.0 eV. Binding energy of Pd($3d_{5/2}$) in Pd metal is at 335.1 eV.[33] This indicates the presence of both +2 and 0 states in the sample reduced at 250 °C. When the same sample is further reduced in $H_2$ at 550 °C, the color turns black. When reduced at higher temperatures, no noticeable change in the color of the reduced sample was observed while transferring to the XPS chamber. Binding energy of Pd($3d_{5/2}$) is shifted to 335.1 eV (Figure 8c),

(30) Powell, C. J.; Larson, P. E. *Appl. Surf. Sci.* **1978**, *1*, 186.
(31) Scofield, J. H. J. *Electron Spectrosc. Relat. Phenom.* **1976**, *8*, 129.
(32) Penn, D. R. J. *Electron Spectrosc. Relat. Phenom.* **1976**, *9*, 29.
(33) Briggs, D.; Seah, M. P. *Practical Surface Analysis*; John Wiley & Sons: New York, 1983.

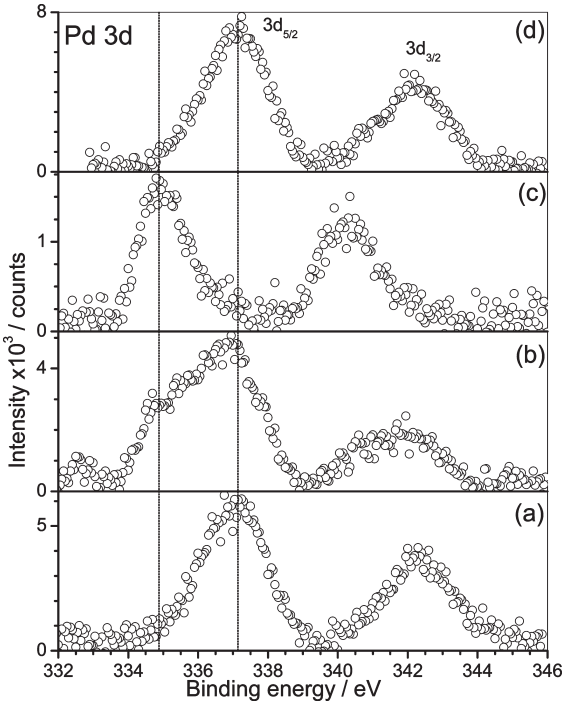


**Figure 8.** Pd 3d core level spectra $Ce_{0.89}Fe_{0.1}Pd_{0.01}O_{2-\delta}$: (a) as-prepared sample, reduced in $H_2$ up to (b) 260 °C, (c) 550 °C, and (d) reoxidized at 550 °C.

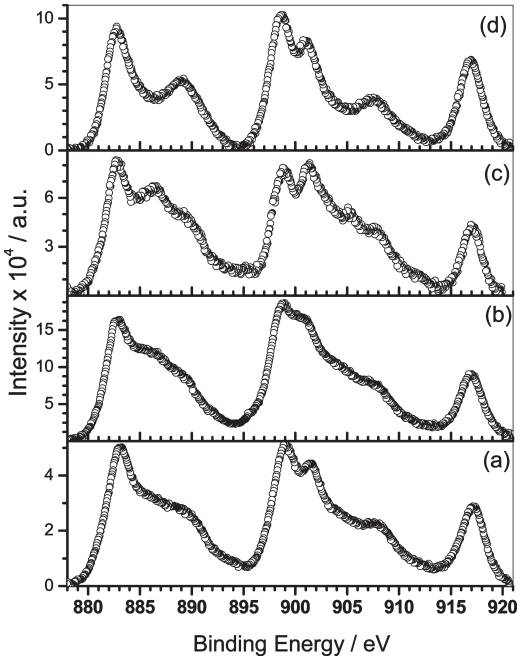


**Figure 9.** Ce 3d core level spectra $Ce0_{.89}Fe_{0.1}Pd_{0.01}O_{2-\delta}$ (a) as prepared sample, reduced in $H_2$ up to (b) 260 °C, (c) 550 °C, and (d) reoxidized at 550 °C.

which indicates that Pd is now completely reduced to $Pd^0$. On reoxidation in $O_2$ at 550 °C Pd gets oxidized to $Pd^{2+}$ state (Figure 8d).

Ce(3d) core level spectra of as prepared $Ce_{0.89}Fe_{0.1}Pd_{0.01}O_{2-\delta}$ is shown in Figure 9a and is found to have 77% of Ce in +4 state and 23% in +3 state. Upon reduction up to 260 °C the $Ce^{3+}$ content was found to increase considerably (Figure 9b) with 70% $Ce^{4+}$ and 30% $Ce^{3+}$ states. On further reduction up to 550 °C, Ce 3d spectra was analyzed to have 65% $Ce^{4+}$ and 35% $Ce^{3+}$ states. On oxidation at 550 °C of the reduced sample, $Ce_{0.89}Fe_{0.1}Pd_{0.01}O_{2-\delta}$ has a higher percentage of Ce in +4 than was originally present in the as-prepared sample with 86% Ce in +4 oxidation state. Bulk reduction of $Fe_2O_3$ to FeO occurs at 545 °C[34] and surface reduction of $CeO_2$ starts at 400 °C,[1] but in the presence of $Pd^{2+}$ ion, reduction of $Fe^{3+}$ to $Fe^{2+}$ and partial $Ce^{4+}$ to $Ce^{3+}$ is brought down to a lower temperature.

In the as-prepared $Ce_{0.89}Fe_{0.1}Pd_{0.01}O_{2-\delta}$, Fe is present in +3 state and Pd in +2 state and 22% Ce is in +3 oxidation state, and therefore its formula is $Ce^{+4}_{0.69}Ce^{+3}_{0.2}Fe^{+3}_{0.1}Pd^{+2}_{0.01}O_{1.84}$. When reduced in $H_2$ at 250 °C, 30% Ce is present in the +3 oxidation state and complete reduction of $Pd^{2+}$ to $Pd^0$ and $Fe^{3+}$ to $Fe^{2+}$ occurs; the formula of the catalyst reduced up to 250 °C is $Ce^{+4}_{0.62}Ce^{+3}_{0.27}Fe^{+2}_{0.1}Pd^{0}_{0.01}O_{1.75}$. When further reduced up to 550 °C, only the Ce reduction is observed and since 35% of Ce in +3 state the formula is given as $Ce^{+4}_{0.58}Ce^{+3}_{0.31}Fe^{+2}_{0.1}Pd^{0}_{0.01}O_{1.73}$.

Relative surface concentrations of Pd and Fe before and after reduction were estimated. The ratio of Pd:Fe:Ce was estimated to be 0.014:0.14:0.845 for the as prepared sample which is close to bulk ratio of 0.01:0.1:0.89. Surface concentration of the reoxidized sample is 0.016:0.13:0.854. Thus, the surface composition of Ce, Fe, and Pd are close to the bulk composition, and ratio does not change upon reduction−oxidation cycle, indicating no surface segregation of any of the ions.

**3.4. $H_2$/TPR and CO/TPR.** *3.4.1. $Ce_{0.9}Fe_{0.1}O_{1.88}$.* The temperature programmed reduction profiles of $Ce_{0.9}Fe_{0.1}O_{1.88}$ (Figure 10 a) shows one broad peak centered at ~400 °C. The TPR of the same sample was carried out for 4 cycles and the redox cycles are reversible. The area under the peak up to 550 °C was used to estimate the oxygen storage capacity (OSC) of the catalyst. OSC of $Ce_{0.9}Fe_{0.1}O_{1.88}$ is found to be 665 $\mu$mol/g, whereas pure $CeO_2$ has an OSC of 350 $\mu$mol $g^{-1}$. Fe is in the +3 oxidation state in the as-prepared sample, as observed from XPS studies, and reduces only to the +2 oxidation state; OSC corresponding to this reduction is 31 $\mu$mol $g^{-1}$. OSC of $Ce_{0.9}Fe_{0.1}O_{1.88}$ is therefore much higher than the sum of same amount of individual $CeO_2$ and $Fe^{3+} \rightarrow Fe^{2+}$ reduction. OSC of $Ce_{0.8}Zr_{0.2}O_2$ is reported to be 533 $\mu$mol/g,[35] which is lower than the OSC of 10% Fe substitution in $CeO_2$. Thus substitution of Fe in $CeO_2$ enhances the reducibility of the oxide, whereby higher percentage of $Ce^{4+}$ to $Ce^{3+}$ reduction could be achieved. The composition of the reduced compound from the TPR data is given as

$$Ce^{+4}_{0.76}Ce^{+3}_{0.14}Fe^{+3}_{0.1}O_{1.88} + 0.11H_2 \rightarrow Ce^{+4}_{0.64}Ce^{+3}_{0.26}Fe^{+2}_{0.1}O_{1.77} + 0.11H_2O \quad (4)$$

(34) Liang, M.; Kang, W.; Xie, K. *J. Nat. Gas Chem.* **2009**, *18*, 110.
(35) Si, R.; Zhang, Y.-W.; Li, S.-J.; Lin, B.-X.; Yan, C.-H. *J. Phys. Chem. B* **2004**, *108*, 12481.

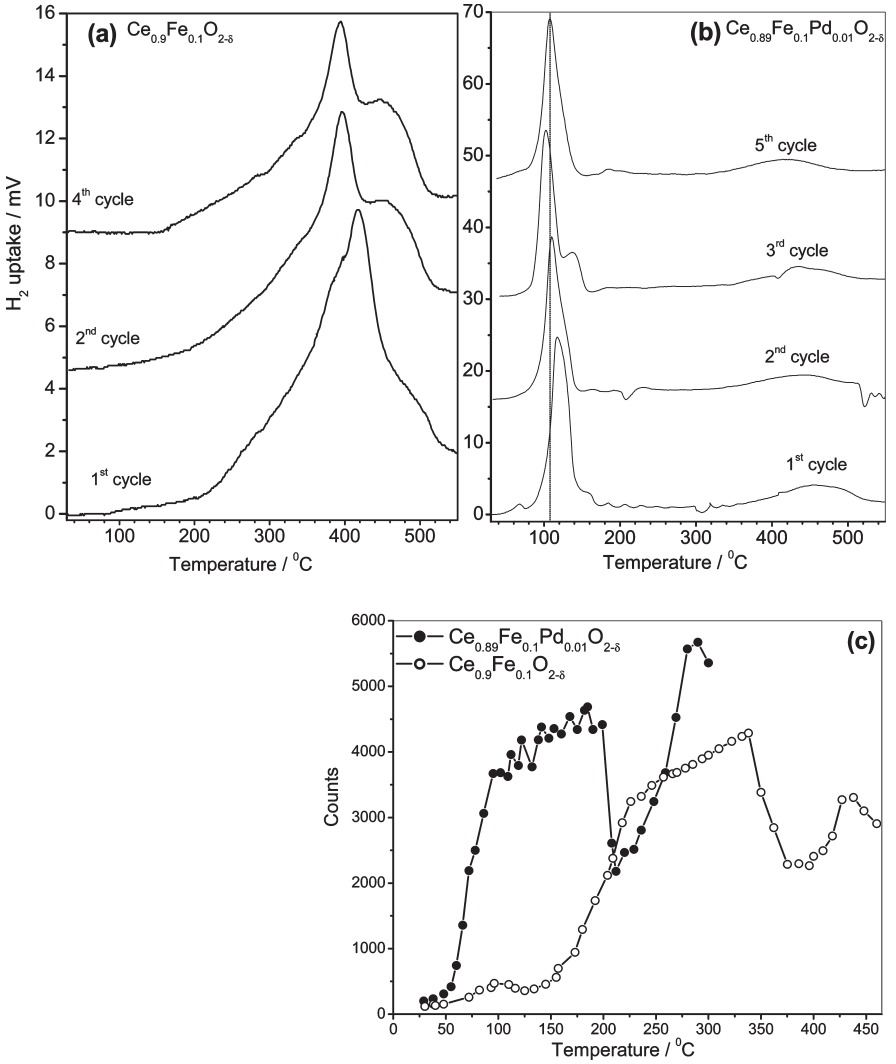


**Figure 10.** $H_2$-TPR profiles of (a) $Ce_{0.9}Fe_{0.1}O_{2-\delta}$, (b) $Ce_{0.89}Fe_{0.1}Pd_{0.01}O_{2-\delta}$, and (c) CO/TPR profiles of $Ce_{0.89}Fe_{0.1}Pd_{0.01}O_{2-\delta}$ and $Ce_{0.9}Fe_{0.1}O_{2-\delta}$.

Composition derived from XPS analysis of the core level Fe 2p and Ce 3d (Table 2) agrees well with the TPR study.

*3.4.2. $Ce_{0.89}Fe_{0.1}Pd_{0.01}O_{1.84}$.* $H_2$/TPR of profiles of $Ce_{0.89}Fe_{0.1}Pd_{0.01}O_{1.84}$ (Figure 10 b) shows a sharp peak around 105 °C and a small peak at ~460 °C. After each cycle, the samples were reoxidized and five TPR runs with the same sample were carried out up to 550 °C. $H_2$/Pd ratio for the $H_2$ uptake peak at 105 °C estimated for all cycle is 9.3, indicating that the $H_2$ uptake reaction is reversible. $H_2$/Pd ratio $>1$ indicates that reduction of $Fe^{3+}$ and $Ce^{4+}$ states is also occurring along with $Pd^{2+}$ to $Pd^0$ reduction; and presence of both $Fe^{2+}$ and $Ce^{3+}$ states were observed in the XPS spectra of the reduced catalyst. Hence substitution of $Pd^{2+}$ ion in $Ce_{0.9}Fe_{0.1}O_{1.88}$ decreases the peak reduction temperature from 400 to 105 °C. OSC corresponding to first reduction peak in the $H_2$/TPR run is calculated to be 592 $\mu$mol/g. The composition of the as-prepared sample is known from XPS analysis and the composition of the reduced catalyst from $H_2$/TPR data is given as

$$Ce^{+4}_{0.69}Ce^{+3}_{0.2}Fe^{+3}_{0.1}Pd^{+2}_{0.01}O_{1.84}+0.09H_2 \rightarrow Ce^{+4}_{0.63}Ce^{+3}_{0.26}Fe^{+2}_{0.1}Pd^{0}_{0.01}O_{1.75}+0.09H_2O \quad (5)$$

When further reduced up to 550 °C the composition of the reduced sample is given as $Ce^{+4}_{0.55}Ce^{+3}_{0.34}Fe^{+3}_{0.1}Pd^{+2}_{0.01}O_{1.71}$. The total OSC up to 550 °C is 780 $\mu$mol $g^{-1}$. Compositions of the as prepared and reduced samples along with XPS composition are given in Table 2. The amount of $Ce^{4+}$ to $Ce^{3+}$ reduction achieved at higher temperatures is very small, corresponding to $\delta \approx 0.01$. The composition derived from XPS analysis agrees with $H_2$/TPR data.

CO/TPR profiles (Figure 10c) of $Ce_{0.9}Fe_{0.1}O_{2-\delta}$ shows CO to $CO_2$ conversion by utilizing lattice oxygen starting at ~200 °C. For Pd ion substituted catalyst, the CO conversion temperature is decreased to ~50 °C, in agreement with $H_2$/TPR results.

Although substitution of Fe activates the lattice oxygen leading to high OSC, with $Pd^{2+}$ ion substitution, activation of lattice oxygen is enhanced with high OSC at substantially low temperature. To gain better insights into this issue of enhanced OSC of $CeO_2$ in the presence of Fe ion, and lower temperature reducibility of Fe-doped $CeO_2$ in the presence of Pd ion, we carried out DFT calculations for these catalysts.

**3.5. DFT Calculations.** To simulate $Ce_{0.9}Fe_{0.1}O_{2-\delta}$ system in a 2 × 2 × 2 supercell model, we replaced four

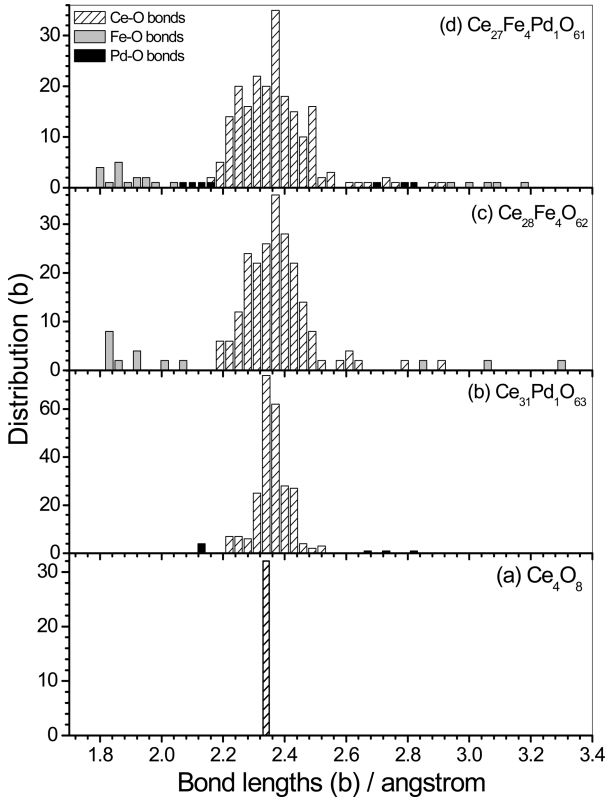


**Figure 11.** Bond lengths distribution of (a) $Ce_4O_8$, (b) $Ce_{31}Pd_1O_{63}$, (c) $Ce_{28}Fe_4O_{62}$, (d) $Ce_{27}Fe_4Pd_1O_{61}$.

Ce atoms with Fe atoms, creating two oxygen vacancies. The formula of the supercell, therefore, is $Ce_{28}Fe_4O_{62}$ corresponding to 12.5% Fe substitution in $CeO_2$, close to experimental composition. To simulate the $Ce_{0.89}Fe_{0.1}$-$Pd_{0.01}O_{2-\delta}$ system, we replaced another Ce atom with a Pd atom, creating an additional oxygen vacancy; therefore, the formula of the supercell is $Ce_{27}Fe_4Pd_1O_{61}$, corresponding to 3.125% Pd substitution. For comparison, $Ce_{0.99}Pd_{0.1}O_2$ and $CeO_2$ was also simulated using a 96-atom $2 \times 2 \times 2$ supercell of $Ce_{31}Pd_1O_{63}$ and 12-atom single unit cell of $Ce_4O_8$, respectively. Simulations of bulk $CeO_2$ (with a $Ce_4O_8$ supercell) was done to minimize the total energy with respect to lattice parameter yielded the theoretical lattice parameter of 5.42 Å, close to the experimental value of 5.41 Å. In the simulations with larger $2 \times 2 \times 2$ supercell, the lattice parameter was kept constant at the value obtained from Rietveld refined XRD pattern, and only the internal atomic positions were optimized to minimize the total energy. The bond lengths derived from the optimized cells are presented Figure 11 in the form of histogram where each bar denotes the number of the bonds in the range equal to the width of the bar. The bond lengths and the coordination number of each element in the supercell are given in Table 3.

Optimized $Ce_4O_8$ unit cell has all Ce−O bond distance equal to 2.34 Å (Figure 11a). For $Ce_{31}Pd_1O_{63}$ supercell Ce−O bonds get distributed over a range of 2.20 to 2.52 Å (Figure 11b), with some of Ce−O getting shorter and some getting longer. The 8-fold coordination of Ce is altered and can be considered approximately as 4 + 4 coordination with four short Ce−O bonds of 2.31 Å and four long Ce−O bonds of 2.38 Å. Pd has 4 + 3 coordination with all the four short Pd−O bonds equal to 2.10 Å (Pd−O bond distance for bulk PdO is 2.02 Å) and three long Pd−O bond lengths range from 2.65 to 2.82 Å, with a mean bond length of 2.72 Å. Thus, Pd ion substitution activates lattice oxygen by the creation of longer Pd−O and Ce−O bonds compared to M−O (M = Pd, Ce) distances in PdO and $CeO_2$. The DFT calculation confirms the activation of lattice oxygen in $Ce_{1-x}Pd_xO_{2-\delta}$ ($x = 0.02$) as observed from $H_2$/Pd ratio of ~2 at 100 °C in $H_2$/TPR experiment.[36]

**Table 3. Coordination Number and Average Bond Lengths**

| compd | cell used for DFT calculation | coordination shell | C.N. | average bond length (Å) |
|---|---|---|---|---|
| $CeO_2$ | $Ce_4O_8$ | Ce−O | 8 | 2.34 |
| $Ce_{0.99}Pd_{0.1}O_{2-\delta}$ | $Ce_{31}Pd_1O_{63}$ | Ce−O | 4 + 4 | 2.31 + 2.38 |
| | | Pd−O | 4 + 3 | 2.11 + 2.72 |
| $Ce_{0.9}Fe_{0.1}O_{2-\delta}$ | $Ce_{28}Fe_4O_{62}$ | Ce−O | 4 + 4 | 2.29 + 2.44 |
| | | Fe−O | 4.5 + 1.5 | 1.88 + 3.06 |
| $Ce_{0.89}Fe_{0.1}Pd_{0.01}O_{2-\delta}$ | $Ce_{27}Fe_4Pd_1O_{61}$ | Ce−O | 4 + 4 | 2.28 + 2.45 |
| | | Fe−O | 4.5 + 1.5 | 1.88 + 2.99 |
| | | Pd-O | 4 + 3 | 2.10 + 2.76 |

**Table 4. Parameters Used for Bond Valence Calculation**

| type of bond | $R_0$ | fitted parameter, $B$ |
|---|---|---|
| Ce−O | 2.117 | 0.326 |
| Fe−O | 1.74 | 0.38 |
| Pd−O | 1.792 | 0.37 |

Optimized supercell of $Ce_{28}Fe_4O_{62}$ shows Ce with 4 + 4 coordination- four O atoms come closer while the other four move away, and with mean short and long Ce−O bond lengths of 2.29 and 2.44 Å respectively(Figure 11c). Of the four Fe atoms, two Fe atoms have 4 + 1 coordination and two Fe atoms have 5 + 2 coordination, with an average CN of Fe of 4.5 + 1.5. The average of short Fe−O bond lengths is 1.88 Å and of long Fe−O bond lengths is 3.06 Å. The short Fe−O bond length (1.88 Å) is close to 1.89 Å for bulk $\gamma$-$Fe_2O_3$.[37] The Ce−O bonds are more distributed in $Ce_{28}Fe_4O_{62}$ and Ce 4 + 4 coordination are more prominent compared to $Ce_{31}Pd_1O_{63}$.

For the $Ce_{28}Fe_4Pd_1O_{61}$ optimized cell, Ce is in 4 + 4 coordination and the mean of the short and long Ce−O bonds is 2.28 and 2.47 Å, respectively; Fe has 4.5 + 1.5 coordination, similar to that of $Ce_{28}Fe_4O_{62}$, and the mean of the short and long Fe−O bond length is 1.88 and 2.99 Å, respectively; Pd has 4 + 3 coordination with mean short and long bond lengths equal to 2.10 and 2.76 Å, respectively (Figure 11d). An interesting feature of the bond-length distribution is that Ce−O bonds are more distributed for $Ce_{27}Fe_4Pd_1O_{61}$ compared to $Ce_{28}Fe_4O_{62}$. From the bond-length distribution, it appears that oxygen bonded with longer Fe−O bonds is more activated than oxygen bonded to Ce and Pd. But oxygen has a tetrahedral coordination in fluorite lattice, and all four bonds of oxygen need to be considered to locate which

(36) Roy, S.; Marimuthu, A.; Hegde, M. S.; Madras, G. *Catal. Commun.* **2008**, *9*, 101.
(37) Liu, T.; Guo, L.; Tao, Y.; Hu, T. D.; Xie, Y. N.; Zhang, J. *Nanostruct. Mater* **1999**, *11*, 1329.

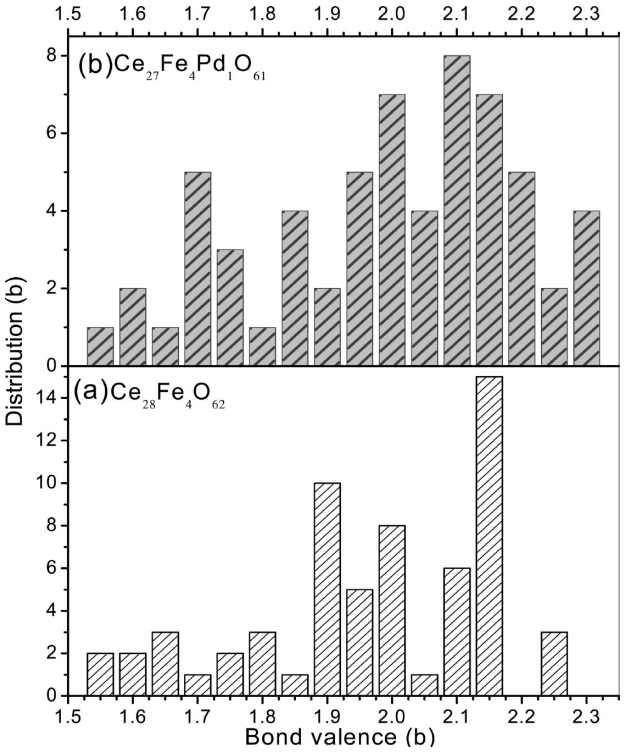


**Figure 12.** Oxygen bond valence distributions of (a) $Ce_{28}Fe_4O_{62}$ and (b) $Ce_{27}Fe_4Pd_1O_{61}$.

oxygen participates in the redox reaction. To understand the weakly bonded oxygen atom, we have carried out bond valence analysis of oxygen.

Bond-valence of Ce and O in $CeO_2$ was calculated to be +3.98 and −1.99, which is close to oxidation state of Ce and O in $CeO_2$. Bond valence distribution of oxygen in $Ce_{28}Fe_4O_{62}$ and $Ce_{27}Fe_4Pd_1O_{61}$ was determined from the oxygen bond distances (shown in Figure 12). The parameters used for bond valence calculation is given in Table 4. Oxygen with 1 short Fe−O and 3 long Ce−O bonds have valency ≈ −1.55 to −1.61, and oxygen with 1 long Fe−O bonds and 3 short Ce−O bonds or 2 short Ce−O and 2 long Ce−O bonds have valency ≈ −1.9 to −2.24. The oxygen that has valency more than 2 is strongly bonded. It has been reported by O'Keeffe and co-workers that oxygen with valency of 1.87 in the Cu−O plane are weakly bonded with the effect that it can be desorbed at ∼ 400 °C. In the present case, oxygen with valency lower than 1.87 can be considered as weakly held in the lattice and can be easily removed under reducing condition.

$Pd^{2+}$ ion substitution shows wider distribution, and bond valence analysis shows more oxygen have lower valency compared to $Ce_{0.9}Fe_{0.1}O_{2-\delta}$ (Figure 12b), implying that more number of oxygen could be extracted from the Pd-substituted catalyst. Thus activation of the lattice oxygen in Fe and Pd substituted $CeO_2$ is due the destabilization of the oxygen sublattic,e leading to distribution of oxygen, some of which forms strong bonds and other weaker bonds.

**3.6. Synergistic Interaction.** From $H_2$/TPR and XPS experiment we have seen that $Fe^{3+}$ and $Ce^{4+}$ ions are

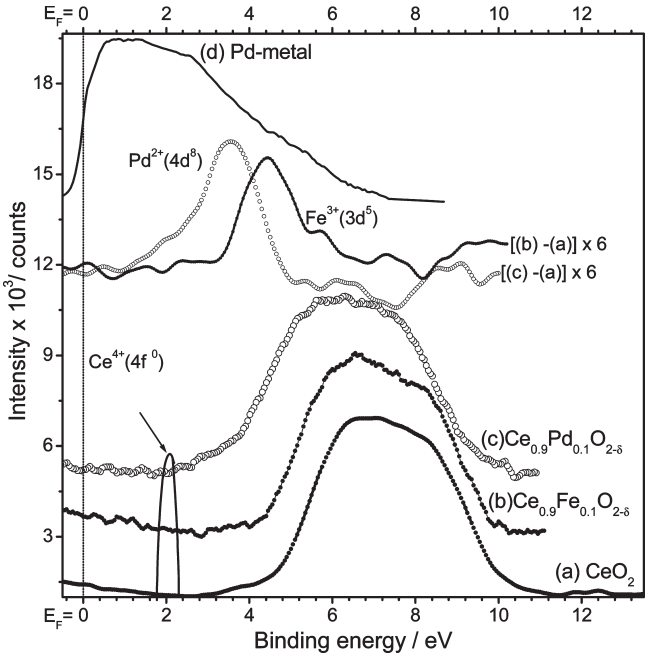


**Figure 13.** Valence band XPS spectra of (a) $CeO_2$, (b) $Ce_{0.9}Fe_{0.1}O_{2-\delta}$, (c) $Ce_{0.9}Pd_{0.1}O_{2-\delta}$ and (d) Pd-metal band. Difference of spectra of (b) − (a) and (c) − (a) multiplied 6 times in $y$-scale.

reduced at ∼105 °C in the presence of Pd ion. PdO reduction by $H_2$ occurs at ∼50 °C,[9] $Fe_2O_3$ reduction in $H_2$ starts from 250 °C,[34] and $CeO_2$ reduction occurs at 450 °C. So at 105 °C, only $Pd^{2+}$ ion reduction is expected, but we observe all $Fe^{3+}$ ions reducing to $Fe^{2+}$ and partial reduction of $Ce^{4+}$ ion to $Ce^{3+}$. This is to be understood from electronic interaction existing between metal ions via oxygen bonds. Valence band region of the catalyst was examined by XPS to understand the mechanism of electronic interaction in the catalyst. The XPS valence band (VB) spectra are shown in Figure 13. The VB spectrum of $CeO_2$ shows occupied density of states of O (2p) starts a ∼3 eV which is consistent with absence of empty 4f level (located ∼2 eV from $E_F$, Fermi level).[38] Position and width of $Fe^{3+}(3d^5)$ and $Pd^{2+}(4d^8)$ bands can be obtained by deducting VB of $CeO_2$ from the valence band of $Ce_{0.9}Fe_{0.1}O_{2-\delta}$ and $Ce_{0.9}Pd_{0.1}O_{2-\delta}$. Accordingly, $Pd^{2+}$-(4d) and $Fe^{3+}$(3d) bands lie at 3.2 and 4 eV respectively from $E_F = 0$. Valence band of Pd metal is also shown in the Figure 13 for comparison. Under reducing $H_2$ atmosphere $Pd^{2+}$ ion reduces to $Pd^0$ as its reduction temperature is the lowest, and $Pd^0(4d^8 + 5s^2)$ band shifts to lower binding energy near to $E_F$ similar to that of Pd metal VB. Because both $Fe^{3+}$ and $Ce^{4+}$ levels lie below the $Pd^0$ band, electron density from $Pd^0$ should be transferred to $Fe^{3+}$ and $Ce^{4+}$ ions

$$Pd^0 + 2Fe^{3+} \rightarrow Pd^{2+} + 2Fe^{2+} \quad (6)$$

$$Pd^0 + 2Ce^{4+} \rightarrow Pd^{2+} + 2Ce^{3+} \quad (7)$$

(38) Sarma, D. D.; Hegde, M. S.; Rao, C. N. R. *J. Chem. Soc., Faraday Trans. 2* **1981**, *77*, 12.

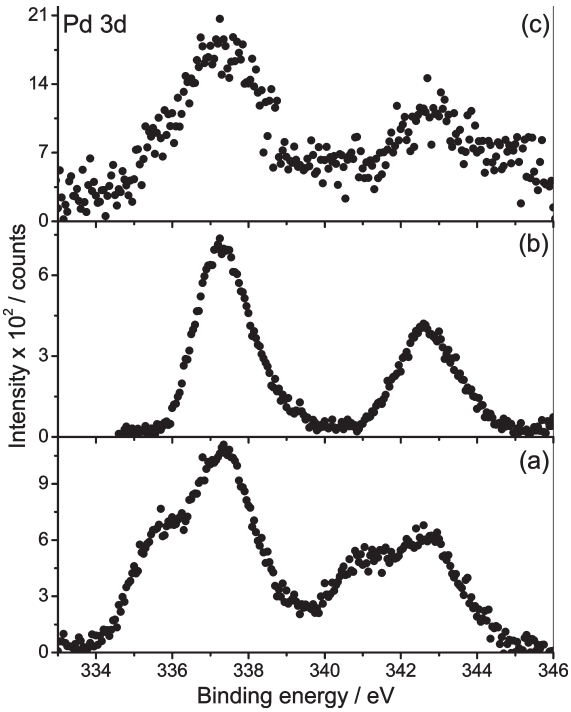


**Figure 14.** Pd 3d core level spectra of (a) as-prepared 3 at % Pd impregnated $Fe_2O_3$, (b) 3 at % Pd impregnated $Fe_2O_3$ heated in Ar at 600 °C for 2 h, (c) 3 at % Pd impregnated $CeO_2$ heated in Ar at 600 °C for 2 h.

To check the feasibility of the above two reactions, we heated 3 at % Pd impregnated $CeO_2$ and $Fe_2O_3$ in Ar at 600 °C for 2 h. Pd (3d) core level XPS of the as prepared impregnated $Fe_2O_3$ and $CeO_2$ sample shows Pd is in both 0 and +2 oxidation state (Figure 14a). Surface of fine Pd metal particles gets oxidized in air while drying the samples at 200 °C. After treatment at high temperatures in Ar, Pd core level spectra of impregnated $Fe_2O_3$ has characteristic binding energy peaks at 337.2 eV corresponding to +2 oxidation state (Figure 14b). Similarly, Pd core level spectra of impregnated $CeO_2$ get oxidized to +2 state after treating at 600 °C (Figure 14C). Thus on heating in Ar, the metallic Pd gets oxidized to $Pd^{2+}$ state in $Fe_2O_3$ and $CeO_2$ by the following redox reaction

$$2xPd^0 + (1-x)Fe_2O_3 \rightarrow Fe_{2-2x}Pd_{2x}O_{3-3x} \quad (8)$$

$$xPd^0 + (1-x)CeO_2 \rightarrow Ce_{1-x}Pd_xO_{2-2x} \quad (9)$$

So when ionic $Pd^{2+}$ is reduced to $Pd^0$ state, the redox coupling between $Pd^0$ and $Ce^{4+}$ and $Fe^{3+}$ via eq 6 and 7 becomes active. $Fe^{2+}$ (3d) band shifts to lower binding energy when $Fe^{3+}$ is reduced by $H_2$ or by $Pd^0$ via eq 7. The resultant $Fe^{2+}$(3d) band lies above $Ce^{4+}$(4f) band (~2 eV) thus reducing $Ce^{4+}$ ion

$$Fe^{2+} + Ce^{4+} \rightarrow Fe^{3+} + Ce^{3+} \quad (10)$$

In $Ce_{0.9}Fe_{0.1}O_{2-\delta}$, the first step of reduction of $Fe^{3+}$ to $Fe^{2+}$ starts from 250 °C and hence the equilibrium (10) is established at high temperature. In the presence of $Pd^{2+}$ ion, the above eqs 6, 7, and 10 occur simultaneously at lower temperature, as observed in $H_2$/TPR and XPS studies. Reduction of the $Ce^{4+}$ and $Fe^{3+}$ state by the $Pd^0$ state is the synergistic interaction due to which low-temperature reduction in $H_2$/TPR experiment is observed.

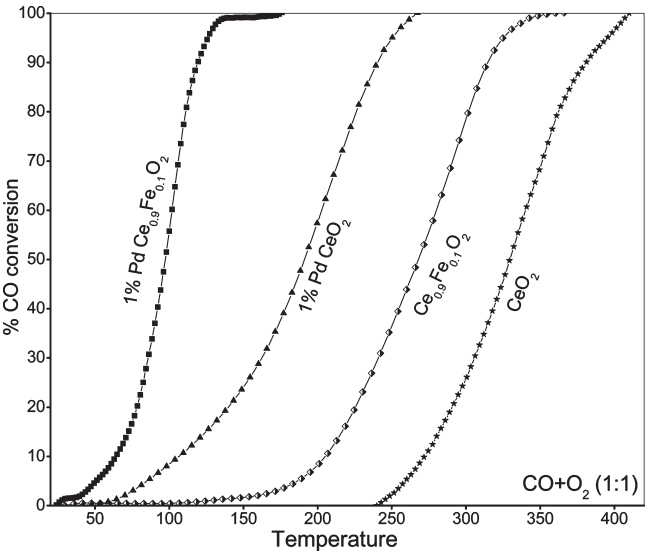


**Figure 15.** Percent CO oxidation by $O_2$ over $CeO_2$, $Ce_{0.99}Pd_{0.01}O_{2-\delta}$, $Ce_{0.89}Fe_{0.1}Pd_{0.01}O_{2-\delta}$ and $Ce_{0.9}Fe_{0.1}O_{2-\delta}$.

**3.7. Catalytic Activity.** *3.7.1. CO Oxidation.* Catalytic CO oxidation over $Ce_{0.99}Pd_{0.01}O_{2-\delta}$, $Ce_{0.9}Fe_{0.1}O_{2-\delta}$, and $Ce_{0.89}Fe_{0.1}Pd_{0.01}O_{2-\delta}$ catalysts in the presence of excess oxygen were carried out and the comparison of the light-off curves are shown in Figure 15. $T_{50}$ (temperature at which 50% conversion is achieved) of CO conversion over $CeO_2$, $Ce_{0.9}Fe_{0.1}O_{2-\delta}$, $Ce_{0.99}Pd_{0.01}O_{2-\delta}$ and $Ce_{0.89}Fe_{0.1}Pd_{0.01}O_{2-\delta}$ are at 330, 260, 190, and 95 °C. Thus $Fe^{3+}$ substitution decreases $T_{50}$ to 260 °C compared to $CeO_2$. $Fe^{3+}$ ion substitution distorts the oxygen sublattice sufficiently, but the electronic transfer between $Fe^{2+}$ and $Ce^{4+}$ is not facilitated at lower temperatures since reduction of $Fe^{3+}$ to $Fe^{2+}$ starts at 250 °C. For $Ce_{0.99}Pd_{0.01}O_{2-\delta}$ catalyst, $T_{50}$ further decreases to 190 °C because electron transfer from $Pd^0$ to the $Ce^{4+}$ state as shown in eq 7 is facilitated. $T_{50}$ further decreases to 95 °C over the bimetal ionic substituted $Ce_{0.89}Fe_{0.1}Pd_{0.01}O_{2-\delta}$ because the presence of $Fe^{3+}$ ion distorts the oxygen sublattice, and electronic transfer is facilitated at low temperature because of the presence of the $Pd^{2+}$ ion. Thus synergistic electronic interaction between the redox couples plays an important role in enhancing CO oxidation activity. Activation energy for catalytic CO oxidation of $Ce_{0.89}Fe_{0.1}Pd_{0.01}O_{2-\delta}$, $Ce_{0.99}Pd_{0.01}O_{2-\delta}$, and $Ce_{0.9}Fe_{0.1}O_{2-\delta}$ is estimated to be 12.5, 15, and 11 kcal/mol.

*3.7.2. NO Reduction by CO Oxidation.* NO reduction by CO over 100 mg catalysts was carried out with the inlet gas flow CO: NO = 1:1 vol % with total gas flow of 100 cc $min^{-1}$. Figure 16 shows the light-off curve of NO reduction by CO and the temperature profiles of $CO_2$, $N_2$, and $N_2O$ formation are given. $T_{50}$ of $Ce_{0.89}Fe_{0.1}Pd_{0.01}O_{2-\delta}$ and $Ce_{0.99}Pd_{0.01}O_{2-\delta}$ is 220 and 180 °C respectively, and

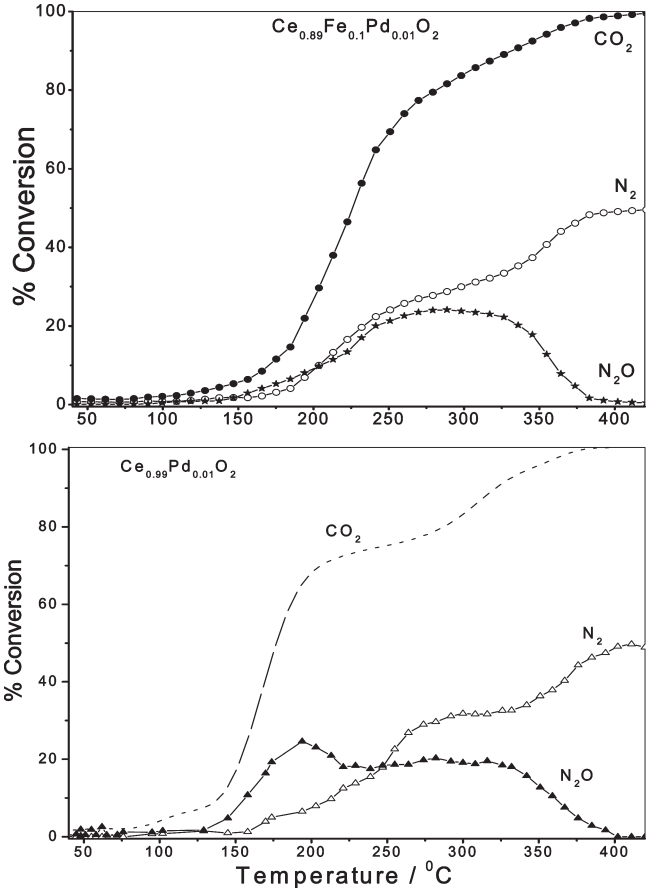


**Figure 16.** Percent NO reduction by CO over (a) $Ce_{0.99}Pd_{0.01}O_{2-\delta}$ and (b) $Ce_{0.89}Fe_{0.1}Pd_{0.01}O_{2-\delta}$.

the corresponding $N_2$ selectivity is 56% and 20%. $T_{50}$ for NO conversion over $Ce_{0.89}Fe_{0.1}Pd_{0.01}O_{2-\delta}$ catalyst is 220 °C which is higher than the $T_{50}$ of 180 °C over $Ce_{0.99}Pd_{0.01}O_{2-\delta}$. But $N_2$ selectivity over $Ce_{0.99}Pd_{0.01}O_{2-\delta}$ catalyst at $T_{50}$ is poor (only 20%) compared to $Ce_{0.89}Fe_{0.1}Pd_{0.01}O_{2-\delta}$ (56%). NO reduction by CO over $Ce_{0.9}Fe_{0.1}O_{2-\delta}$ catalyst occurs at high temperature, with $T_{50}$ at 360 °C (not shown in the figure) and $N_2$ selectivity at $T_{50}$ is also very poor ~9%. Hence $Ce_{0.89}Fe_{0.1}Pd_{0.01}O_{2-\delta}$ is a good catalyst in terms of $N_2$ selectivity, and though $T_{50}$ is higher compared to that in $Ce_{0.99}Pd_{0.01}O_{2-\delta}$, 100% NO reduction and CO oxidation over both the catalyst occurs at the same temperature of 380 °C.

*3.7.3. NO Reduction by $H_2$.* To study NO reduction by $H_2$, we have taken 2% Pd substituted catalyst instead on 1% Pd substituted catalyst. The light-off curve for NO conversion is shown in Figure 17. The $T_{50}$ (the temperature of 50% conversion) of NO conversion over the catalysts $Ce_{0.88}Fe_{0.1}Pd_{0.02}O_{2-\delta}$, $Ce_{0.98}Pd_{0.02}O_{2-\delta}$, and $Ce_{0.9}Fe_{0.1}O_{2-\delta}$ are at 140, 180, and 350 °C, respectively. Bimetal ionic ion substituted $CeO_2$ is a good catalyst for

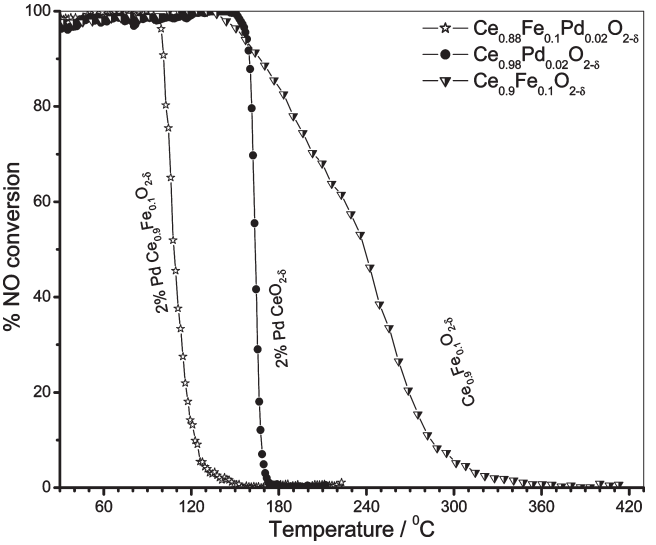


**Figure 17.** Light off curve of % NO reduction by $H_2$ over $Ce_{0.88}Fe_{0.1}Pd_{0.02}O_{2-\delta}$, $Ce_{0.9}Fe_{0.1}O_{2-\delta}$ and $Ce_{0.98}Pd_{0.02}O_{2-\delta}$.

NO reduction by $H_2$ compared to the monometal-ionic substituted $CeO_2$.

## 4. Conclusion

(1) Nanocrystalline $Ce_{0.9}Fe_{0.1}O_{2-\delta}$ and $Ce_{0.89}Fe_{0.1}Pd_{0.01}O_{2-\delta}$ solid solution, synthesized by novel combustion method, exhibit high oxygen storage/release property (OSC) compared to $CeO_2$.

(2) From $H_2$/TPR and XPS studies, the presence of active redox couples $Pd^{2+}/Pd^0$, $Fe^{3+}/Fe^{2+}$ and $Ce^{4+}/Ce^{3+}$ has been identified. Presence of $Pd^{2+}$ ion in $Ce_{0.89}Fe_{0.1}Pd_{0.01}O_{2-\delta}$ brings down the temperature of $H_2$-uptake peak considerably compared to $Ce_{0.9}Fe_{0.1}O_{2-\delta}$.

(3) From DFT calculations, it is found that the oxygen sublattice is highly distorted in $Ce_{0.9}Fe_{0.1}O_{1.88}$ and $Ce_{0.89}Fe_{0.1}Pd_{0.01}O_{1.84}$ compared to $CeO_2$ and $Ce_{0.99}Pd_{0.1}O_{2-\delta}$, leading to formation of long and short M−O (M = Fe, Pd, Ce) bonds. Presence of longer oxygen bonds decreases the oxygen bond valence to approximately −1.5, leading to activation of lattice oxygen, which in turn is responsible for high the OSC property observed in the catalysts.

(4) Reduction of $Pd^{2+}$ to $Pd^0$ and simultaneous reduction of $Ce^{4+}$ to $Ce^{3+}$ and $Fe^{3+}$ to $Fe^{2+}$ states by $Pd^0$ is the synergistic interaction responsible for high OSC at low temperature observed in bimetal ionic catalyst $Ce_{0.89}Fe_{0.1}Pd_{0.01}O_{1.84}$ compared to monometallic $Ce_{0.9}Fe_{0.1}O_{1.88}$ and $Ce_{0.99}Pd_{0.01}O_{2-\delta}$.

**Acknowledgment.** We thank the Department of Science and Technology, Government of India, for financial support. We thank the central computing facility at JNCASR for use of computational resources.